[24]H. Kahlert and G. Bauer, Phys. Status Solidi 46(b), 535 (1971).
[25]G. Bauer and H. Kahlert, Phys. Rev. B 5, 566 (1972).
[26]J. Kolodziejczak, Acta Phys. Polon. 20, 289 (1961).
[27]W. Zawadzki and W. Szymanska, J. Phys. Chem. Solids 32, 1151 (1971).
[28]E. J. Johnson and D. H. Dickey, Phys. Rev. B 3, 2676 (1970).
[29]A. Arnaud and G. Quentin, Phys. Letters 32A, 16 (1970).
[30]M. Hass, in *Semiconductors and Semimetals*, edited by R. K. Willardson and A. C. Beer (Academic, New York, 1967), Vol. 3, p. 14.
[31]S. Zwerdling, W. H. Kleiner, and J. P. Theriault, J. Appl. Phys. Suppl. 32, 2118 (1961).
[32]R. R. L. Zucca and Y. R. Shen, Phys. Rev. B 3, 2668 (1970).
[33]D. Matz, Phys. Rev. 168, 843 (1968).
[34]L. M. Roth and P. N. Argyres, in *Semiconductors and Semimetals*, edited by R. K. Willardson and A. C. Beer (Academic, New York, 1966), Vol. 1, p. 159.
[35]L. M. Bliek, G. Landwehr, and M. v. Ortenberg, in *Proceedings of the International Conference on the Physics of Semiconductors, Moscow* 1968, edited by S. M. Ryvkin (Nauka, Leningrad, 1969), p. 710.
[36]J. J. Whalen and C. R. Westgate, J. Appl. Phys. 43, 1965 (1972).
[37]R. S. Crandall, Solid State Commun. 7, 1575 (1969).
[38]K. W. Nill and A. L. McWhorter, J. Phys. Soc. Japan Suppl. 21, 755 (1966).
[39]G. Arlt and P. Quadflieg, Phys. Status Solidi 25, 323 (1968).
[40]I. L. Drichko, Y. V. Ilisavskii, and Y. M. Galperin, Fiz. Tverd. Tela 11, 2463 (1969) [Sov. Phys. Solid State 11, 1989 (1970)].
[41]W. D. Smith, J. G. Miller, R. K. Sundfors, and D. I. Bolef, J. Appl. Phys. 42, 2579 (1971).
[42]D. L. Rode, Phys. Rev. B 2, 1012 (1970).
[43]D. Kranzer and E. Gornik, Solid State Commun. 9, 1541 (1971).
[44]V. V. Galavanov, D. N. Nasledov, and A. S. Filipchenko, Phys. Status Solidi 8, 671 (1965).
[45]F. Buchy, Phys. Status Solidi 10, K3 (1965).
[46]E. Haga and H. Kimura, J. Phys. Soc. Japan 18, 777 (1963).
[47]S. M. Puri, Phys. Rev. 139, A995 (1965).
[48]S. Tanaka, S. Asai, and M. Kogami, in Ref. 35, p. 779.
[49]S. Zukotynski, S. Graf, and N. Saleh, Phys. Status Solidi 42, K43 (1970).
[50]D. Long, Phys. Rev. 99, 388 (1955).
[51]S. Doniach, Proc. Phys. Soc. (London) 73, 849 (1959).
[52]R. A. Stradling and R. A. Wood, J. Phys. C 3, 2425 (1970).
[53]G. P. Alldredge and F. J. Blatt, Ann. Phys. (N. Y.) 45, 191 (1967).

PHYSICAL REVIEW B VOLUME 7, NUMBER 6 15 MARCH 1973

Brillouin-Scattering Study of Propagating Acoustoelectric Domains in Semiconducting CdS†

Masayoshi Yamada,* Chihiro Hamaguchi, Kazuhisa Matsumoto, and Junkichi Nakai
Department of Electronics, Faculty of Engineering, Osaka University, Suita, Osaka, Japan
(Received 2 March 1972; revised manuscript received 7 July 1972)

Brillouin scattering in an anisotropic medium is developed by taking account of the off-axis effect, and some aspects of amplified shear waves in propagating acoustoelectric domains in semiconducting CdS are presented. The small-signal theory for piezoelectrically active waves amplified from the thermal background of lattice vibrations is formalized by taking account of nonelectronic lattice loss. When the acoustic flux intensity was less than about 10^{-3} J/cm^3, the growth rate and frequency dependence of the on-axis components of acoustic flux were all found to be consistent with the small-signal theory. As for the off-axis components, the angular distribution of the acoustic flux, angular dependence of net gain coefficient, and narrowing of the cone of the acoustic flux also gave a reasonably good agreement with the theory. However, they have been strongly subjected to the influence of the nonelectronic-lattice-loss term. Using a dual-pulse method, it was found that the frequency dependence of the attenuation of acoustic flux was proportional to $f^{1.5}$ and its angular dependence proportional to the square of the off-axis angle. The angular dependence of the nonelectronic lattice loss was tentatively explained with the help of boundary scattering. In the subsequent stages of growth, when the acoustic waves became very intense, many interesting nonlinear effects were found in contrast to the small-signal theory. The acoustic spectrum was rapidly extended to both low and high frequencies, compared with that as expected under the small-signal condition. The subharmonic was strongly amplified and its growth rate became three times larger than that of initially amplified flux. There was a reasonably large growth rate even at high frequencies.

I. INTRODUCTION

It is well known that energy and momentum are transferred from the mobile charge carriers to the acoustic waves when the drift velocity exceeds the sound velocity by the application of a sufficiently high electric field.[1,2] The electrical instabilities caused by such interactions of electrons or holes with internally generated acoustic waves have been observed in many piezoelectric semiconductors[3]

(CdS,[4] CdSe,[5] CdTe,[6] ZnO,[7] ZnS,[8] GaAs,[9] GaSb,[10] InSb,[11] Te,[12] and $Se_{10}Te_{90}$[13]). These instabilities are generally classified into two types of current patterns: continuous and damped oscillations. The former is characterized by a high-field domain which propagates with the velocity of sound in the direction of carrier drift, while the latter is characterized by a stationary domain located at either the downstream contact or an inhomogeneity in the bulk of the sample. The behavior and nature of such domains were investigated by means of various methods: electrical probe,[14,15] transmission of microwave radiation,[16,17] rotation of the polarization plane of light,[18,19] and transmission of light near the intrinsic absorption edge.[20-22] Brillouin scattering is a more powerful method than those mentioned above to study the strong acoustic flux in the domain, and hence the amplification process of the acoustic flux through the acoustoelectric interactions between mobile carriers and internally generated acoustic waves. Such investigations in semiconducting CdS, where the piezoelectric interactions are stronger, have been reported by many authors.[23-32] However, these studies were primarily limited to the final stages in growth of the acoustic waves, assuming a direction for the constituent acoustic wave (usually taken to be the direction of the applied electric field).

It has been recently found in Brillouin-scattering experiments in GaAs that all observed properties of the acoustic flux initially detected are consistent with linear amplification of shear waves present in the equilibrium thermal background.[33-35] In the case of CdS, however, such detailed measurements and investigations have not yet been reported. With these situations in mind we tried to study the amplification of the acoustic flux from the thermal background in CdS by Brillouin-scattering measurements. We took the birefringence and off-axis effect of propagating acoustic flux into account explicitly.

This paper aims mainly to confirm the applicability of small-signal theory, to point out some evidence of the appropriateness of parametric conversion[30,36] for the deviation from it, and to obtain the information about the nonelectronic lattice loss. When more than a single wave with a strong intensity are present, interactions occur between the different waves, which result in nonlinear interactions. To distinguish the strong nonlinear interaction from the linear interaction, we shall call the former the "strong-flux regime" and the latter the "weak-flux regime" (or "linear"). Since the strong-flux regime is very complicated, we develop here a linear theory which is valid in the weak-flux regime. In the present experiment, the exponential growth was observed during the period from the onset of the current drop through half-way toward its saturation level. The exponential growth was found to break down after this period, and instead strong subharmonic flux was detected.

We begin our discussion in Sec. II by deriving expressions for the weak-flux regime. The theory developed in this section is an extension of the analysis made by Spears.[34] The theory takes the frequency and angular distribution into account and the acoustic-energy density amplified from the thermal background is estimated in order to compare it with the present experiment. In Sec. III, Brillouin scattering in an anisotropic material is examined by taking account of the birefringence and the off-axis effect, and the experimental method is presented. The experimental results are divided into three parts; in Sec. IV A, the behavior of on-axis acoustic waves, such as frequency spectrum and growth rate, is given; in Sec. IV B the results for off-axis acoustic waves are given; and in Sec. IV C the results for the nonelectronic lattice loss as a function of frequency and propagation direction are given.

II. THEORY

Because of the strong variation of the acoustoelectric gain with the frequency and propagation direction of the acoustic wave, the amplification is restricted to a small portion of the thermal spectrum of piezoelectrically active shear waves propagating in a relatively narrow cone. In the present experiments, the direction of the electric field is perpendicular to the c axis of the CdS crystals, and therefore only the shear waves are amplified. In the following analysis we apply the theory developed by Spears[34] to the case of CdS.

Taking into account the lattice-loss term, we get the net-gain coefficient in the following form:

$$\alpha_n(\vec{q}) = \alpha_{HW}(\vec{q}) - \alpha_l(\vec{q}), \tag{2.1}$$

where $\alpha_{HW}(\vec{q})$ is the acoustoelectric-gain coefficient and $\alpha_l(\vec{q})$ the nonelectronic-ultrasonic-attenuation coefficient, both of which depend on the wave vector of phonons $\vec{q}$. If $ql_e \ll 1$(where l_e is the electron mean free path), the gain coefficient is given by the Hutson–White theory. The loss term $\alpha_l(f)$ varies as f^2 for $\omega\tau_{th} \ll 1$, and f for $\omega\tau_{th} \gg 1$, where $f = \omega/2\pi$ is the frequency of the ultrasonic waves and τ_{th} is the thermal-phonon relaxation time.[37] Since $\alpha_l(f)$ increases monotonically with f, the frequency of maximum net gain, f_n, is always less than the frequency of maximum gain, $f_0 = (\omega_C\omega_D)^{1/2}/2\pi$ (where ω_C is the dielectric relaxation frequency and ω_D is the diffusion frequency), and decreases with decreasing the drift velocity.[38] The frequency distribution of Eq. (2.1) may be expanded around f_n as was done by Spears.[34] Then

we obtain

$$\alpha_n(f) = \alpha_n(f_n)\{1 - p[(f-f_n)/f_n]^2\}, \quad (2.2)$$

where p is constant.

Now we consider the angular dependence of Eq. (2.1) and we define a coordinate system in which the z axis is the c axis of the crystal and the x axis is the direction of electron drift. The propagation direction of the waves makes an angle η with respect to the C plane (x-y plane), and its projection onto the C plane forms an angle δ with respect to the x axis. If a wave is propagating in the C plane ($\eta = 0$), the piezoelectric, elastic, and dielectric constants are constant, while, if $\eta \neq 0$, they are dependent on η.[39] An additional factor occurs in the drift-velocity component $v_d \cos\delta \cos\eta$. As revealed by the present experiments, the lattice loss α_l parabolically depends on the propagation direction. Therefore, we assume the following relation:

$$\alpha_l(\delta, \eta) = \alpha_l(0)(1 + A_\delta \delta^2 + A_\eta \eta^2), \quad (2.3)$$

where A_δ and A_η are constants. It should be kept in mind that the parabolic dependence of α_l plays an important role in the narrowing of the cone. Finally, we obtain for the angular dependence of the net gain approximately

$$\alpha_n(\delta, \eta) = \alpha_n(0)(1 - Q_\delta \delta^2 - Q_\eta \eta^2), \quad (2.4)$$

where Q_δ and Q_η are constants. In the present case,

$$Q_\delta = [0.5\alpha_0\gamma(1 + 1/\gamma) + A_\delta \alpha_l(f_0)]/\alpha_n, \quad (2.5)$$

$$Q_\eta = [\alpha_0\gamma(9.5 + 1.25/\gamma) + A_\eta \alpha_l(f_0)]/\alpha_n. \quad (2.6)$$

Taking into account the angular and frequency dependence described above, the total excess energy density within bandwidths near $f = f_n$ and $\delta = \eta = 0°$ may be estimated through the same procedure as Spears's.[34] The result is

$$\Phi(t) \simeq \frac{C_n k T}{v_s^3} f_n^2 \left\{\frac{\pi f_n^2}{p\alpha_n t}\right\}^{1/2} \left[\frac{\pi}{Q_\delta \alpha_n t}\right]^{1/2} \left[\frac{\pi}{Q_\eta \alpha_n t}\right]^{1/2} e^{\alpha_n t}, \quad (2.7)$$

when p, Q_δ, and Q_η are much greater than $1/\alpha_n t$. The quantity in the curly brackets is the effective frequency bandwidth $\Delta f_{1/2}$, and the terms in the square brackets are the effective cone of propagation $\Delta\delta_{1/2}\,\Delta\eta_{1/2}$. Equation (2.7) indicates that these bandwidths of the amplified beam will be decrease as the flux grows. At the 10^6 growth stage, we found that $\Delta f_{1/2} \simeq 1$ GHz and $\Delta\delta_{1/2} \simeq 10°$ in a typical sample of semiconducting CdS.

III. ANISOTROPIC BRILLOUIN SCATTERING AND EXPERIMENTAL PROCEDURE

Brillouin scattering is capable of resolving the frequency and wave-vector components of the acoustic flux through accurate measurements of the frequency and angular dependence of the scattered-light intensity. It is generally known that Brillouin scattering from a transverse acoustic wave has the property that the diffracted light is polarized at right angles to the polarization of the incident light.[40] In our measuring case where the transverse acoustic wave with its displacement along the c axis propagates in the C plane, the anisotropic Bragg diffraction law[41,42] must be used, taking into consideration that the refractive index of the incident optical polarization differs from that of the diffracted polarization. The conservation law of momentum and Snell's law lead to useful relations of the external incident angle θ_i' and the external diffracted angle θ_d' with the frequency and propagation angle δ of phonons:

$$\theta_i' = \sin^{-1}\left\{n_i \sin\left[\sin^{-1}\frac{\lambda_0}{2n_i v_s} \times\left(f + \frac{v_s^2}{f\lambda_0^2}(n_i^2 - n_d^2)\right) + \delta\right]\right\}, \quad (3.1)$$

$$\theta_d' = \sin^{-1}\left\{n_d \sin\left[\sin^{-1}\frac{\lambda_0}{2n_d v_s} \times\left(f - \frac{v_s^2}{f\lambda_0^2}(n_i^2 - n_d^2)\right) - \delta\right]\right\}, \quad (3.2)$$

where $n_i (= n_0 = 2.460$[43]$)$ is the refractive index of the incident optical polarization, $n_d (= n_e = 2.477$[43]$)$ is the index of the diffracted polarization, $v_s (= 1.75 \times 10^5$ cm/sec$)$ is the velocity of the transverse sound wave of interest, and $\lambda_0 (= 6328$ Å$)$ is the wavelength of the light in free space. A measurement of the scattered intensity at the angle θ_i' and θ_d' uniquely determines the phonon intensity of f and δ, when the volume of $\vec{q}$ space probed by the light beam falls well within the cone of the amplified phonon beam.

Next we consider the scattering intensity factor. In the case of GaAs, Spears has found that multiple scattering has an appreciable effect on the scattering signal for intense scattering.[34] In the present experiment, however, multiple-scattering signals were not observed. Therefore we neglect the multiple-scattering process for simplicity. We assume that the intensity of the light, dI_s, scattered while propagating a distance between y and $y + dy$ is given by

$$dI_s = I_0 \sigma_t\, dy\, e^{-\sigma_t y} \quad (3.3)$$

for weak scattering ($\sigma_t y \ll 1$), where I_0 and σ_t are the intensity of the incident light (at $y = 0$) and the total scattering coefficient.[34] Since we are dealing with the case of weak scattering, we have to take into account multiple internal reflections of both scattered and unscattered light beams. With this in mind, the intensity of the scattered light can be easily obtained:

$$\frac{I_s}{I_0} \simeq \sigma_i b \frac{1+R_{\parallel}(\theta_i')R_{\perp}(\theta_d')}{[1+R_{\parallel}(\theta_i')][1+R_{\perp}(\theta_d')]} \frac{n_0}{(n_0^2-\sin^2\theta_i')^{1/2}}$$
$$\equiv \sigma_i b \beta, \tag{3.4}$$

where we define β as a scattering intensity factor, and where b is the sample thickness, $R_{\parallel}(\theta_i')$ the reflectivity for the incident light polarized parallel to the plane of incidence, and $R_{\perp}(\theta_d')$ the reflectivity for the scattered light polarized perpendicular to the plane of incidence. When the incident angle θ_i' increases beyond Brewster's angle $\theta_B = 68°$, the reflectivity $R_{\parallel}(\theta_i')$ increases sharply. Therefore the intensity decreases very rapidly with increasing θ_i', for $\theta_i' > \theta_B$. This limits the frequency observed by Brillouin scattering. In the on-axis case, $\delta = 0°$, β is flat over the range of frequencies from 150 MHz to 4.5 GHz.

Our experimental setup is similar to those reported elsewhere.[23,30,34] The scattering jig which we used consists of a goniometer head Y845 (Enraf Nonius, Delft) and a scattering table (Shimadzu, Japan) with two rotatable arms around a vertical axle. A He-Ne laser with the output power about 1 mW was used as a light source. Horizontally polarized light emitted from the light source was focused to about 0.2 mm in diameter. The scattered light was detected by an RCA 7265 photomultiplier through an analyzer and an aperture A_s defining the collection cone Ω' (< 0.02 sr was used in the present experiment). The collection cone Ω' limits the resolution. If we employ a fixed collection cone, the frequency resolution is higher in both lower- and higher-frequency regions, while the propagation-direction resolution is higher in the higher-frequency region and lower in the lower-frequency region. The sample was mounted by soldering the wires to the output terminals on the goniometer head without any other supports.

The samples were cut in bar shapes from the ingots of semiconducting CdS single crystals purchased from Eagle Picher Co., and mechanically or chemically polished. In order to obtain Ohmic contacts, indium was evaporated on the ends of the sample at 1×10^{-5} Torr, and copper wires were soldered on them with an indium-gallium compound. The dimensions (length × thickness × height), carrier concentrations (n), and mobilities (μ) of five samples used are listed in Table I, together with the frequency (f_0) of the maximum acoustoelectric gain calculated from the Hutson–White theory. The carrier concentration and mobility were determined by the persistent acoustoelectric currents.[44] Although most samples exhibited large variations in resistivity measured by the detailed optical-probe technique,[45] some of them exhibited small variations in resistivity. Such specimens with good homogeneity were used for quantitative analysis in the present work.[46]

IV. RESULTS AND DISCUSSIONS

A. Spectral Composition and Growth Rate

The best test of the growth was provided by Brillouin-scattering measurements on samples from the ingot UHP 7, where a 2.8-GHz acoustic wave produced the most intense scattering at the initial stages of detection. The intensity of this wave was measured as a function of time for six different applied fields. The net-gain coefficient $\alpha_n(f_n)$ may be estimated from the simple exponential-growth range of each growth curve. A plot of $\alpha_n(f_n)$ versus applied field E_0 is shown in Fig. 1, which yields the parameters α_0 ($\equiv \frac{1}{4}K_{15}^2\omega_D$, where K_{15} is the electromechanical coupling constant) and $\alpha_t(f_n)$. At 2.8 GHz, we find $\alpha_t = 3\times10^6$ sec^{-1}, which is reasonably consistent with that obtained from another adequate experiment as shown later. In addition, we find $\alpha_0 = 40\times10^6$ sec^{-1}, which is in good agreement with the small-signal Hutson–White theory, according to which we obtain $\alpha_0 = 43.6\times10^6$ sec^{-1} with the electromechanical coupling constant $K_{15}^2 = 0.037$.

In the weak-flux regime, the frequency distribution of the amplified flux at a time 2.1 μsec after the application of the field (860 V/cm) on a UHP-7.2 sample is shown by the data points in Fig. 2, along with the energy distribution of the shear waves in thermal equilibrium, calculated according to the theory developed in Sec. II for a 1-GHz bandwidth and 10° propagation cone. We found that the maximum net-gain coefficient is about 5.4×10^6 sec^{-1} at the above field, with the acoustic flux around 2.8 GHz producing the most intense scattering at the initial stage of detection. The energy

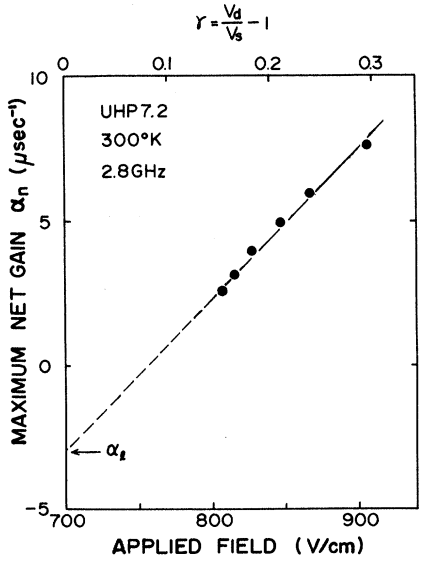

FIG. 1. Net gain coefficient α_n vs applied field E_0. The parameter $\gamma = v_d/v_s - 1$ is also given.

TABLE I. Dimensions (length× thickness× height) and electrical properties of CdS at room temperature. The height of the sample is parallel to the c axis. The calculated frequency of maximum acoustoelectric gain is also given.

Sample No.	Dimensions (mm)	n (cm^{-3})	μ ($cm^2\ V^{-1}\ sec^{-1}$)	f_0 (GHz)
UHP 7.2	10.08×0.30×1.66	2.7×10^{15}	250	4.0
UHP 7.3	10.75×0.54×1.40	2.8×10^{15}	270	4.1
UHP 10.11	9.55×0.57×0.82	2.7×10^{15}	300	4.0
UHP 10.12	9.55×0.90×0.82	2.7×10^{15}	300	4.0
UHP 10.13	9.55×1.30×0.82	2.7×10^{15}	300	4.0

density at the stage shown by the data points is estimated to be about 4.2×10^{-5} J/cm^3, which is 2×10^5 times the thermal background. The curve denoted α_{HW} represents the amplified spectrum calculated by the Hutson–White theory using the present sample parameters. The theory without the loss term gives about a 10^4–10^5 times larger flux level than was experimentally observed. The lattice losses drop the amplified energy density remarkably and produce a downward shift in the frequency of the maximum intensity. As will be described in Sec. IV C, we found from another experiment that the lattice loss varies as $\alpha_l \propto f^{1.5}$, with 5.5×10^6 sec^{-1} for the frequency $f=4$ GHz (see Fig. 9). If the nonelectronic-loss term is included in the analysis as described in Sec. II, we have the frequency of maximum net gain, $f_n=3$ GHz, and the net-gain coefficient $\alpha_n=5.3\times10^6$ sec^{-1}, which are in good agreement with the experimentally observed values $f_n=2.8$ GHz and $\alpha_n=5.4\times10^6$ sec^{-1}, respectively. The amplified spectrum calculated by taking the nonelectronic lattice loss into account is demonstrated by a curve denoted by $\alpha_{HW}-\alpha_l$ in Fig. 2. As seen in this figure, the small-signal theory developed in Sec. II, where the initial flux is assumed to be the thermal background, is in good agreement with the values measured here in the weak-flux regime.

Figure 3 shows an example of the normalized scattering intensities as a function of time for

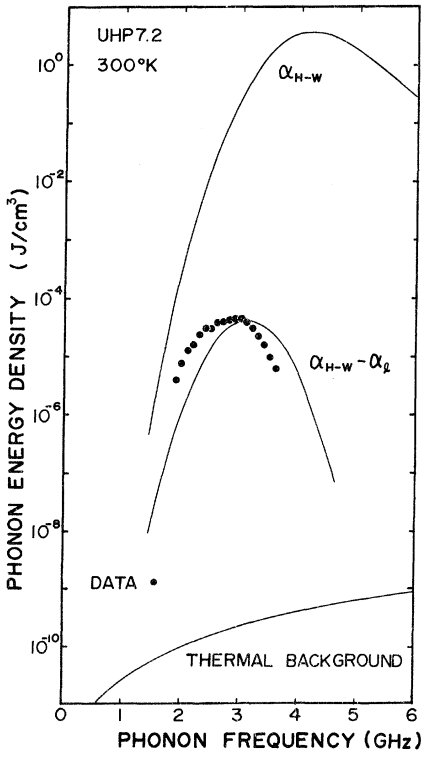

FIG. 2. Frequency distribution of the amplified acoustic energy density at an early growth stage. The solid curves represent the thermal background intensity and the theoretical amplified distributions (see discussions in text).

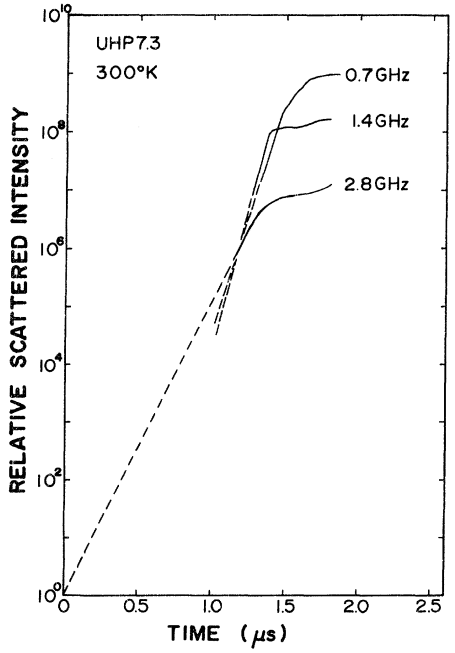

FIG. 3. Relative scattering intensity as a function of time for the 2.8-, 1.4-, and 0.7-GHz acoustic waves.

three different frequencies: f_n, $\frac{1}{2}f_n$, and $\frac{1}{4}f_n$, for the specimen UHP 7.3. The effective thermal-energy density U_{th} may be given by the extrapolation of the simple exponential-growth range for the 2.8-GHz flux back to $t=0$. The intensity of the fundamental flux starts to saturate at the growth stage of 10^7 times U_{th}, where the energy density is estimated to be an order of 10^{-3} J/cm^3 using the data obtained in the present work; that is, the net-gain coefficient $\alpha_n = 1.2\times10^7$ sec^{-1}, the frequency bandwidth 1 GHz, and the effective cone angle 10°. The decrease in growth rate and the onset of flux saturation imply the end of the simple exponential growth or of the small-signal region. The applicability of the simple gain theory is attested up to such flux level. Assuming constant drift velocity, the excess electric field obtained from the ratio of momentum transfer[47] from the mobile charge carriers to the amplified acoustic waves is given by[34]

$$E_d(t) - E_0 = (nev_s)^{-1}\int \alpha\phi_{\vec{q}}(t)d\vec{q} \simeq \alpha\Phi(t)/nev_s , \tag{4.1}$$

where $E_0 = v_d/\mu$ is the Ohmic field in the absence of the amplified acoustic flux and $E_d(t)$ the local electric field in the presence of the flux. At the growth stage of 10^7U_{th} (about 10^{-3} J/cm^3), the peak excess electric field in the domain $(E_d - E_0)$ estimated from Eq. (4.1) is about 300 V/cm. It should be noted that the results of Figs. 1 and 2 were obtained under the condition of $E_d - E_0 \ll E_0$. At the onset of saturation of the fundamental flux (2.8 GHz), the frequency spectrum was observed to spread to lower frequencies and subharmonics (1.4 and 0.7 GHz) became of comparative strength, which indicates the onset of strong nonlinear effects. The subharmonic flux grows up about three times faster than the flux of the fundamental frequency (2.8 GHz). The saturation level of these subharmonics is higher than that of the fundamental frequency and their saturation energy densities may be roughly estimated of orders of 10^{-2}–10^{-1} J/cm^3. The saturation values of the fundamental and subharmonic fluxes in CdS are slightly smaller than those measured in GaAs.[34] There is also an interesting difference in the subharmonic generation: The intensity of the subharmonics in CdS becomes comparable with the fundamental flux well before the fundamental flux saturates, while in GaAs it is comparable only after the fundamental flux saturates completely.

The rapid and delayed growth of the subharmonics indicate that the flux does not grow up through the amplification mechanism from the thermal background predicted by the small-signal theory. It may be due to parametric down conversion; that is, the two-frequency model of parametric-subharmonic conversion proposed by Zemon *et al.*[36,48] However, it should be noted that the phonon amplified from the thermal background (the pumping source) does not consist of acoustic waves with single frequency and fixed propagation direction, but of acoustic waves with a certain bandwidth of frequency and propagation cone.

The frequency spectra of the relative scattering intensity at three stages in growth are shown in Fig. 4, as an example of the deviation from the small-signal theory. The spectrum at a time $t = 1.3$ μsec is in reasonable agreement with the small-signal theory. At subsequent stages ($t = 1.4$ and 1.5 μsec) the distribution broadens on low- and high-frequency sides. The broadening on the low-frequency side is remarkable. It should be noted that the data shown are scattering intensity, not energy density, and that a frequency-sensitive correction must be made to convert these data into energy density.[49] Although the spectra at the latter two stages are broad, a second peak appears at about one-half the frequency of the first peak. Such a large shift in the peak cannot be explained from the small-signal theory.

Figure 5 shows the net-gain coefficients in the frequency region 0.5–4 GHz, which are obtained from the slope of the growth curve. The net-gain coefficients on both low- and high-frequency sides are larger than the values expected by the small-signal theory. We find that the net gain at about $\frac{1}{2}f_n$ is three times larger than that at f_n. This fact is explained well by the parametric amplification. The amplification of higher frequencies is not much higher than the value expected from the small-signal theory. This may be explained by the

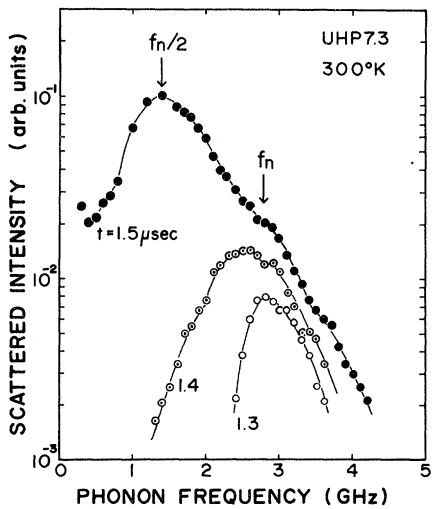

FIG. 4. Frequency spectra of the relative scattering intensity at three different stages in growth. The frequency of maximum net gain f_n and the second subharmonic $\frac{1}{2}f_n$ are indicated by the arrows.

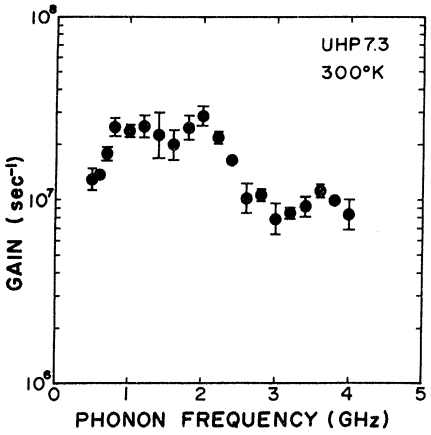

FIG. 5. Experimentally determined net gains $\alpha_n(f)$ as a function of frequency. Note that the gains except for the vicinity of the frequency of maximum net gain ($f = 2.8$ GHz) are obtained in the strong-flux regime. The higher gain at lower frequencies is a consequence of the parametric down conversion.

fact that the higher nonelectronic lattice loss suppresses the amplification at higher frequencies.

B. Angular Distribution of Amplified Phonon

The angular distribution in the C plane of the frequency of maximum net gain (2.8 GHz) at four stages of growth is shown in Fig. 6. The distribution is Gaussian and its center is slightly shifted from 0°. We cannot find what has caused the shift; perhaps, the misinstallment of the sample or the inherent behavior of the amplified phonon in this sample. We found the center of the amplified phonon was very close to 0° in another specimen. We find in Fig. 6 a gradual shift to 0° in the peak with time. Three stages at $t = 1.2$, 1.3, and 1.4 μsec are in a linear growth range. It is interesting to note that the flux around the center of the distribution is growing up, while the flux around both edges saturates or decreases at the last stage, i.e., shrinkage of the propagation cone of flux expected from the small signal theory. The angular bandwidth of the 2.8-GHz flux is about 10° in the weak-flux regime and becomes narrower as the intensity of the flux increases. In the strong-flux regime, it is 5°–6°. Similar narrowing of the cone angle for the 1.4-GHz subharmonic flux is also observed, as will be seen in Fig. 7. The shrinkage is from 7° to 4° in the observable range of the scattering signal.

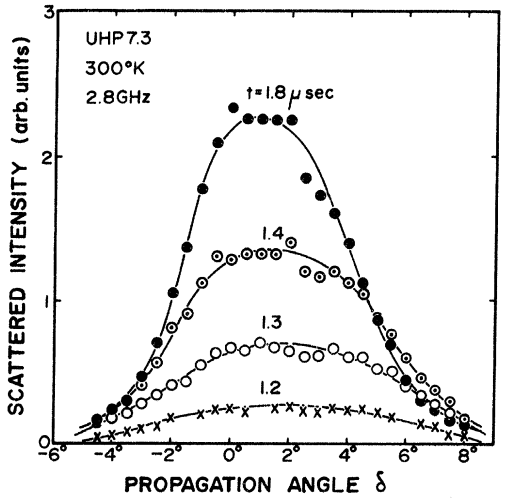

FIG. 6. Angular distribution for the 2.8-GHz acoustic flux in the C plane at four different stages in growth. Note that the shrinkage of the angular cone occurs during these stages.

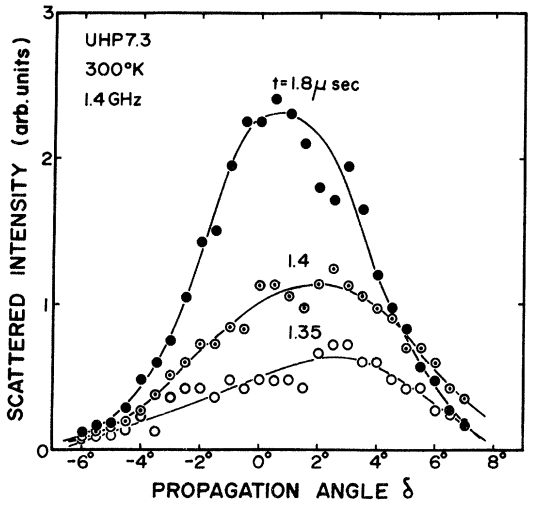

FIG. 7. Angular distribution of the 1.4-GHz acoustic flux in the C plane at three different stages in growth. Note that the unsymmetrical distribution of the flux is indicative of subharmonic conversion.

Figure 7 shows the angular distribution of the 1.4-GHz subharmonic flux at three growth stages. The distribution at the early stage is remarkably warped in comparison to the fundamental flux. At the last stage, it becomes a Gaussian form. The distribution peak is considerably shifted from 0° at the early stage to then approach 0° more rapidly than the fundamental flux. At the early stages two peaks seem to be found at 0° and 3°. The difference in the peak positions is indicative of subharmonic conversion. The substantial transfer of energy from the pump to the signal and idler through the parametric-subharmonic conversion requires that the waves are at least approximately phase matched, i.e., the three wave vectors form a closed triangle. At the later stage $t = 1.8$ μsec, however, those two peaks disappear, and the angular distribution has a Gaussian character. The half-width for the 1.4-GHz flux is slightly

smaller than that for the 2.8-GHz flux. In the strong-flux regime, where strong flux of subharmonics exists, the parametric-subharmonic and -harmonic conversions take place through the interactions between substantially amplified fluxes of f_n, $\frac{1}{2}f_n$, and so on, which consist of certain bandwidths of frequency and angular cone. Thus the distribution becomes a Gaussian character.

The angular distribution of net gain in the C plane is shown in Fig. 8 for the $f_n = 2.8$-GHz flux, along with the theoretical curves calculated according to the Hutson–White theory with (denoted $\alpha_{HW} - \alpha_l$) and without the contribution from the nonelectronic lattice loss (denoted by α_{HW}). The data points have been obtained from the slope of the exponential-growth range for each off-axis component. The propagation angle for the maximum net gain is about 2°. Its deviation from 0° might be perhaps caused by the misorientation of the c axis. The net-gain coefficient varies parabolically with respect to the propagation angle, as expected from the Hutson–White theory, where the drift-velocity component ($v_d \cos\delta$) only influences the angular distribution of gain, since the electromechanical coupling coefficient is constant in the C plane, as stated in Sec. II. There exists no quantitative agreement between the experimental values and the theoretical values calculated by using α_{HW}, where the theoretical curve is shifted by 2° with respect to the propagation angle in order to fit with the data. We obtain a good agreement between the experimental and theoretical values if we take the nonelectronic lattice loss into account, where we assumed parabolic variation for the angular dependence of the lattice loss as mentioned in Sec. II and as experimentally confirmed later (see Figs. 10 and 11). The contribution of the lattice loss term to the parabolic behavior of net gain is 4 times larger than that of the drift-velocity component, and the constant Q_6 that appeared in Eq. (2.5) is about 12 with δ in radians.

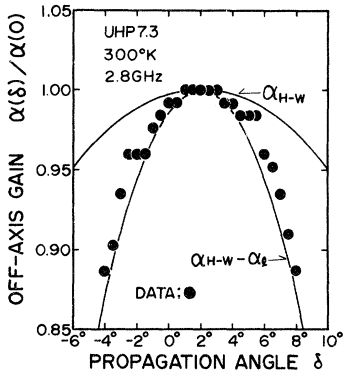

FIG. 8. Net gain coefficient as a function of the propagation direction for the 2.8-GHz acoustic flux. Also shown are the theoretical curves calculated from the Hutson–White theory with $\alpha_{HW} - \alpha_l$ and without the loss term α_{HW} (see discussions in text).

C. Frequency and Angular Dependence of Lattice Loss

In the measurements of the lattice loss, we have employed the dual-pulse method as described by Zucker *et al.*,[50] where a longer (~5 μsec) pulse V_1 served as the control for the sample bias current in order to maintain the condition $v_d = v_s$, while a shorter (~1 μsec) pulse V_2 was superimposed on the longer pulse to generate the acoustic flux. The relative intensity of the acoustic flux was monitored with Brillouin scattering at a point in the sample such that the arrival time of the acoustic packet occurred during the flat-top of V_1 but after the turnoff of V_2. The application of the V_2 pulse was limited so that the excitation of the acoustic flux might be as weak as possible.

Figure 9 shows the frequency dependence of the attenuation coefficient α_l of the UHP 7.2 sample measured under the condition that the electron-drift velocity equal to the sound velocity. We find in this sample that the frequency dependence of α_l is approximately given by $f^{1.5}$ with a value of about 0.7×10^6 sec^{-1} at 1 GHz. The lattice-loss coefficient α_l around f_n is comparable to the value estimated from the net-gain coefficient stated in Sec. IV A. This frequency dependence gives a reasonable agreement with that measured at frequencies from 90 to 480 MHz by Bateman and McFee,[51] using the pulse-echo method, where a pulse acoustic flux of a single frequency was excited in the photoconductive specimen by a nonresonant transducer. However, Zucker *et al.*[50] observed in measurements similar to the present experiment that the lattice loss varies as $\alpha_l \propto f$. In the present work we also observed similar behavior in the specimen UHP 7.3. The difference in the frequency dependence of the lattice loss is not clear at the present stage of the experiments. It should be noted that the measured loss term is influenced by the boundary scattering especially in the region of low frequencies.[52]

For CdS at room temperature, the thermal-conductivity measurement yields $\tau_{th} = 7\times10^{-12}$ sec.[53] Thus, at $f = 1$ GHz, $\omega\tau_{th} = 0.044$, and the $\omega\tau_{th} \ll 1$ limit should be applied. In such a region, theories predict α_l as varying as f^2. The ultrasonic wave has a very long wavelength compared to the mean free path of the thermal phonon; it is more instructive to consider the ultrasonic wave as a perturbation on the lattice waves, rather than as being scattered by the waves. There are a number of theories which give similar frequency and temperature dependences for the attenuation.[37,54] The general feature of these theories is that they give a linear dependence of the attenua-

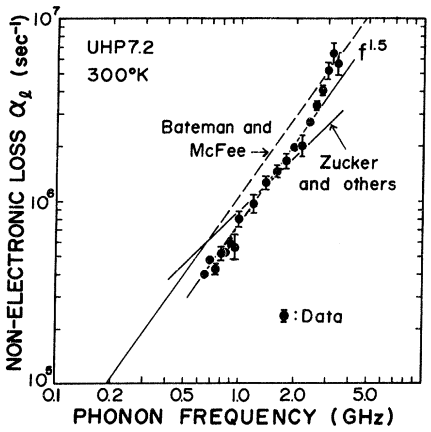

FIG. 9. Frequency dependence of attenuation coefficient for on-axis acoustic waves measured under the condition $v_d = v_s$.

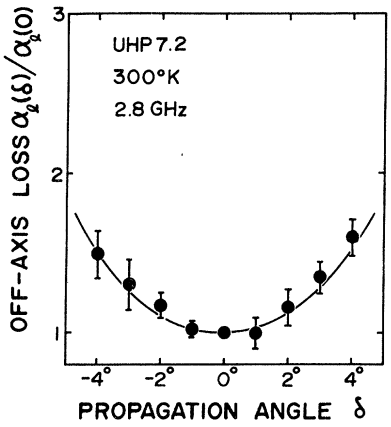

FIG. 10. Angular dependence of attenuation coefficient for the 2.8-GHz flux measured under the condition of $v_d = v_s$.

tion on τ_{th} and ω^2; that is, $\alpha_l \propto \omega^2 \tau_{th}$. However, a survey of other materials, except for Ge and some alkali halides,[54] reveals departures from an f^2 dependence at 300 °K in the GHz frequency range. The departures have received relatively little attention in the literature, though Miller[55] has pointed out that a strong frequency dependence for τ_{th} itself gives a deviation from f^2 dependence.

Our measuring method differs from that of the usual attenuation of a monochromatic and coherent beam of phonons, because there are phonons of many frequencies and random phases grown up from the thermal background through the acoustoelectric amplification process. Therefore, it is not obvious whether the usual theory of ultrasonic attenuation is applicable or not.

As stated in Sec. IV B, the angular dependence of the net gain cannot be explained without the assumption that the lattice loss has a strong angular dependence. This stimulated us to investigate the angular dependence of the lattice-loss coefficient. The same method as used in the frequency dependence was employed. In such a method, an additional term arises from the acoustoelectric-gain factor which contains $v_d \cos\delta$ and the sound velocity. In the C plane, however, the sound velocity is constant. Thus we take account of the angular dependence of the drift-velocity factor only. Since $\alpha_0 = 4.3 \times 10^7$ sec^{-1} and $\alpha_l = 3.3 \times 10^6$ sec^{-1} at 2.8 GHz in the sample UHP 7.2, the factor $|\alpha_0(\cos\delta - 1)|/\alpha_l$ is less than 5% in the range of the present experiment ($|\delta| < 5°$). Thus we conclude that the measured loss term excludes the contribution from the gain term.

Results are presented in Figs. 10 and 11 for the 2.8- and 1.4-GHz fluxes, respectively. The lattice loss of off-axis components varies parabolically with respect to the propagation angle at both frequencies. The angular dependence is found to be stronger at 1.4 than at 2.8 GHz. The parabolic coefficient A_δ of the nonelectronic lattice loss is 100 for the 2.8-GHz flux and 200 for the 1.4-GHz flux in this sample. It is difficult to explain why the lattice attenuation should have a strong off-axis dependence. The only possibility to explain this behavior is the boundary scattering.[56] Off-axis flux, even in an angle of only a few degrees, must strike the side surfaces of the sample, unless the sample has a very thick cross section. If the flux striking the various surfaces is not specularly reflected, this represents a loss mechanism. The greater the off-axis angle, the more flux is lost through such side effects. At the lower frequency, the true lattice attenuation is weaker, so any surface effect would appear to be stronger. This explains why the effect seems to be stronger at 1.4 than at 2.8 GHz.

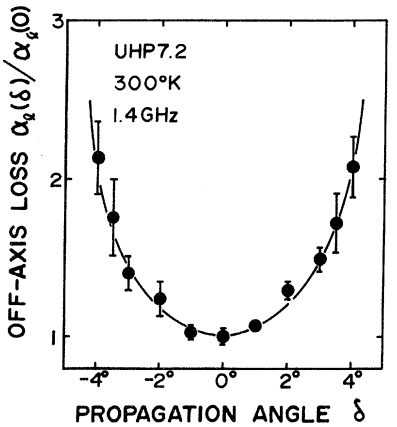

FIG. 11. Angular dependence of attenuation coefficient for the 1.4-GHz flux measured under the condition of $v_d = v_s$.

The nonelectronic lattice loss defined from measurements on a particular specimen depends on the shape of the crystal and on the smoothness of the surface, when the size of the specimen is comparable with the mean free path of the phonons. This was examined by estimating the value of A_δ for specimens with different cross sections. The results are shown in Fig. 12, where the coefficient A_δ is plotted as a function of the thickness. The coefficient A_δ increases markedly with decreasing thickness. This indicates that the boundary scattering plays an important role in the loss mechanism, especially for a specimen with smaller cross section. A tentative explanation for the parabolic behavior of the loss term is given in the Appendix by taking into account the boundary scattering.

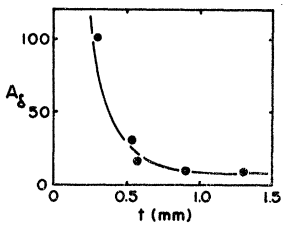

FIG. 12. Parabolic coefficient A_δ of nonelectronic lattice loss for the 2.8-GHz acoustic flux vs sample thickness t.

ACKNOWLEDGMENTS

The authors are very grateful to Professor R. Bray for many valuable suggestions, and to Dr. N. Mikoshiba and Dr. H. Ozaki for helpful comments. We are also indebted to Professor U. Kubo for loan of a He-Ne laser at an early stage of this experiment. One of the authors (C. H.) is pleased to acknowledge valuable discussions with Professor R. Bray and Dr. D. L. Spears during his stay at Purdue University.

APPENDIX: BOUNDARY SCATTERING OF PHONONS

Since the surface roughness of our samples, which were polished with alumina powder of 0.3 μm in diameter, is comparable with the wavelength of phonons (0.625 μm for 2.8 GHz and 1.25 μm for 1.4 GHz) measured in the present investigation, and since the cross section of the sample is not thick enough, we have to consider the effect of the boundary scattering on the loss term. We cannot treat them as either perfectly rough or perfectly smooth surfaces. We employ a simple phenomenological description, according to the treatment of Ziman.[57] We assume that a fraction $p(\delta)$ of the incident phonons are specularly reflected, as if by a highly polished mirror, while the remainder are scattered diffusely in all directions uniformly. This fraction $p(\delta)$ has been statistically calculated by Ziman as the following:

$$p(\delta) = e^{-\pi\phi^2} = e^{-16\pi^3\xi^2 \sin^2\delta/\lambda^2}, \tag{A1}$$

where ξ is the root-mean-square deviation of the height of the surface from a reference plane, and λ is the wavelength of the incident wave.

If $p(\delta)\neq 0$, then we must take the multiple reflection of phonons into account. In such a case, we have the mean free path for boundary scattering,

$$\Lambda_B = [(1+p)/(1-p)]\Lambda_{0B}, \tag{A2}$$

where Λ_{0B} is the value for perfectly rough surfaces, which is equal to the equivalent sample diameter L. If the boundary scattering and the internal scattering are additive in their effects, then we obtain

$$1/\Lambda = 1/\Lambda_i + 1/\Lambda_B \tag{A3}$$

for the total mean free path Λ, where Λ_i is the mean free path associated with the internal scattering. Using the well-known relation between the mean free path and the lifetime, we have from Eqs. (A1)–(A3)

$$\frac{\alpha_l(\delta)}{\alpha_l(0)} = 1 + \frac{8\pi^3\xi^2 v_s}{L\lambda^2\alpha_l(0)}\sin^2\delta \simeq 1 + A_\delta\delta^2 \tag{A4}$$

for the normalized off-axis loss.

Assuming that $\xi \sim 0.5$ μm, we have $A_\delta \simeq 200$ for the acoustic wave of $f = 1.4$ GHz, which is consistent with our measured value. However, we have to note that the above treatment cannot explain the frequency dependence of the coefficient A_δ. Since $\alpha_l(0) \propto f^{1.5}$, we obtain the result $A_\delta \propto f^{0.5}$ in contrast to the experimental result. The above treatment is valid for the 1.4-GHz flux where we have $\xi < \lambda$. For the 2.8-GHz flux, we have $\xi \simeq \lambda$, and the present analysis is not valid.

---

†Work supported by the Hattori Hokokai Foundation.

*The partial support of Iue Memorial Scholarship for M. Y. is greatly appreciated.

[1]A. R. Hutson, J. H. McFee, and D. L. White, Phys. Rev. Letters 7, 237 (1961).

[2]D. L. White, J. Appl. Phys. 33, 2547 (1962); A. R. Hutson and D. L. White, *ibid.* 33, 40 (1962).

[3]For reviews of acoustoelectric domain phenomena, see R. Bray, IBM J. Res. Develop. 13, 487 (1969); in *Proceedings of the Tenth International Conference on the Physics of Semiconductors*, edited by S. P. Keller, J. C. Hensel, and F. Stern (Atomic Energy Commission, Oak Ridge, Tenn., 1970), p. 705; J. Yamashita and K. Nakamura, *ibid.*, p. 694; and N. I. Meyer and M. H. Jørgensen, in *Festkörper Probleme X*, edited by O. Madelung (Vieweg, Braunschweig, Germany, 1970), p. 21.

[4]R. W. Smith, Phys. Rev. Letters 9, 87 (1962).

[5]M. Kikuchi, Japan. J. Appl. Phys. 2, 12 (1963).

[6]M. Kikuchi, Japan. J. Appl. Phys. 4, 233 (1965).

[7]J. H. McFee, J. Appl. Phys. 34, 1548 (1963).

[8]W. E. Spear and P. G. Le Comber, Phys. Rev. Letters 13, 434 (1964).
[9]H. Ikoma, I. Kura, and K. Hataya, J. Phys. Soc. Japan 19, 141 (1964).
[10]P. O. Sliva and R. Bray, Phys. Rev. Letters 14, 372 (1965).
[11]J. B. Ross and R. Bray, Bull. Am. Phys. Soc. 11, 173 (1966).
[12]G. Quentin and J. M. Thuiler, in *Proceedings of the Seventh International Conference on the Physics of Semiconductors, Paris*, 1964, edited by M. Halin (Academic, New York, 1964), p. 571.
[13]T. Shiosaki, H. Matsumoto, K. Kinugawa, and A. Kawabata, Japan. J. Appl. Phys. 10, 1491 (1971).
[14]J. H. McFee, P. K. Tien, and H. L. Hodges, J. Appl. Phys. 38, 1721 (1967).
[15]W. H. Haydl, K. Harker, and C. F. Quate, J. Appl. Phys. 38, 4295 (1967).
[16]E. Pohlendt and W. Wettling, Phys. Letters 25A, 22 (1967).
[17]M. Bruun and N. I. Meyer, Phys. Letters 26A, 493 (1968).
[18]H. J. Fossum and A. Rannested, J. Appl. Phys. 38, 5177 (1967).
[19]Y. Mita, J. Appl. Phys. 42, 2886 (1971).
[20]C. S. Kumar, P. O. Sliva, and R. Bray, Phys. Rev. 169, 680 (1968).
[21]K. Yamamoto, M. Yamada, and K. Abe, J. Appl. Phys. 41, 450 (1970).
[22]K. Yamamoto, M. Yamada, and K. Abe, J. Phys. Soc. Japan 29, 1521 (1970).
[23]J. Zucker and S. Zemon, Appl. Phys. Letters 9, 398 (1966); 10, 212(E) (1967).
[24]S. Zemon, J. H. Wasko, L. L. Hope, and J. Zucker, Appl. Phys. Letters 11, 40 (1967).
[25]W. Wettling, Phys. Letters 25A, 193 (1967).
[26]W. Wettling and M. Bruun, Phys. Letters 27A, 123 (1968).
[27]B. W. Hakki and R. W. Dixson, Appl. Phys. Letters 14, 185 (1969).
[28]A. Ishida and Y. Inuishi, J. Phys. Soc. Japan 26, 957 (1969).
[29]W. Wettling and M. Bruun, Phys. Status Solidi 34, 221 (1969).
[30]S. Zemon and J. Zucker, IBM J. Res. Develop. 13, 494 (1969).
[31]M. Bruun, W. Wettling, and N. I. Meyer, Phys. Letters 31A, 31 (1970).
[32]M. Asdente, M. Musci, and G. Randone, Phys. Letters 33A, 475 (1970).
[33]D. L. Spears, IBM J. Res. Develop. 13, 499 (1969).
[34]D. L. Spears, Phys. Rev. B 2, 1931 (1970).
[35]E. D. Palik and R. Bray, Phys. Rev. B 3, 3302 (1971).
[36]S. Zemon, J. Zucker, J. H. Wasko, E. M. Conwell, and A. K. Ganguly, Appl. Phys. Letters 12, 378 (1968).
[37]M. G. Holland, IEEE Trans. Sonics Ultrasonics SU-15, 18 (1968).
[38]A. R. Hutson, Phys. Rev. Letters 9, 296 (1962).
[39]N. F. Foster, G. A. Coquin, G. A. Rozgonyi, and F. A. Vannatta, IEEE Trans. Sonics Ultrasonics SU-15, 28 (1968).
[40]R. W. Gammon, in *Light Scattered Spectra of Solids*, edited by G. B. Wright (Springer, New York, 1969), p. 579.
[41]R. W. Dixson, IEEE J. Quantum Electron. QE-3, 85 (1967).
[42]L. L. Hope, Phys. Rev. 166, 883 (1968).
[43]T. M. Bieniewski and S. J. Czyzak, J. Opt. Soc. Am. 53, 496 (1963).
[44]D. L. Spears and R. Bray, Phys. Letters 29A, 542 (1969).
[45]M. Yamada, C. Hamaguchi, and J. Nakai, Japan. J. Appl. Phys. 10, 1541 (1971).
[46]In Brillouin-scattering measurements, additional inhomogeneity arises from the laser-induced photoconductivity. Since we employed a low-power laser (1 mW) and used the highly conductive specimen ($\sim 0.2/\Omega$ cm) in our present experiments, there was little change in the total conductivity. Therefore, we believe that the irradiation of laser has no influence on homogeneity. However, a high-power laser (15 mW) gave a little change in the total conductivity.
[47]G. Weinreich, Phys. Rev. 107, 317 (1957).
[48]E. M. Conwell and A. K. Ganguly, Phys. Rev. B 4, 2535 (1971).
[49]See Ref. 34. In the case of CdS, however, analysis of resolution is quite complicated due to the birefringence of this material. In the present experiment a He-Ne laser was used as an incident light source and therefore the collection aperture limited the resolution rather than angular spread of the incident light. In the case of on-axis acoustic waves, the frequency resolution is relatively flat and is less than 300 MHz, while the resolution of propagation direction varies from 5° to 1° within the observed frequency range from 500 MHz to 4 GHz.
[50]J. Zucker, S. A. Zemon, and J. H. Wasko, in *Proceedings of the Ninth International Conference on the Physics of Semiconductors*, edited by S. M. Ryvkin (Nauka, Leningrad, 1968), p. 904.
[51]T. B. Bateman and J. H. McFee, J. Appl. Phys. 39, 4471 (1968).
[52]Recently we found from Brillouin scattering in photoconducting CdS with a large cross section that the angular cone is about 15° at $f_n = 250$ MHz, which is much larger than that obtained in semiconducting CdS. This might indicate that the angular cone depends on the cross section of the specimen owing to the boundary scattering.
[53]M. F. Lewis, J. Acoust. Soc. Am. 43, 852 (1968).
[54]For a review, see M. Pomerantz, Proc. IEEE 53, 1438 (1965).